



Chitosan-mediated facile green synthesis of size-controllable gold nanostars for effective photothermal therapy and photoacoustic imaging



Thi Tuong Vy Phan^a, Van Tu Nguyen^b, Seok-Hwan Ahn^{d,*}, Junghwan Oh^{c,e,*}

^a Center for Advanced Chemistry, Institute of Research and Development, Duy Tan University, Da Nang 550000, Viet Nam

^b Interdisciplinary Program of Biomedical Mechanical & Electrical Engineering, Pukyong National University, Busan 48513, Republic of Korea

^c Center for Marine-Integrated Biomedical Technology, Pukyong National University, Busan 48513, Republic of Korea

^d Department of Aero Mechanical Engineering, Jungwon University, Chungbuk 28024, Republic of Korea

^e Department of Biomedical Engineering, Pukyong National University, Busan 48513, Republic of Korea

ARTICLE INFO

Keywords:

Green synthesis
Gold nanostars
Chitosan
Photothermal therapy
Photoacoustic imaging

ABSTRACT

With the large near-infrared (NIR) absorption and the high NIR photothermal effect, gold nanostar (AuNS) has potential application in the biomedical field. However, the complicated synthesis process with toxic precursors is a serious issue for its practice. Herein, we reported a novel green synthesis procedure using chitosan polymer from marine and vitamin C for the preparation of AuNS. For the first time, chitosan was used as a stabilizer, shape-directing, and size-controllable agents for the preparation of AuNS. The size of the obtained AuNS ranged from 111 to 225 nm with different λ_{max} . The AuNS exhibited near-infrared absorption with the excellent biocompatibility toward non-cancerous cell line (MG63) and cancerous cell line (MDA-MB-231). The *in vitro* photothermal therapy and photoacoustic imaging with assisting of obtained AuNS were also proved the high efficiency of these nanoparticles.

1. Introduction

Photothermal therapy (PTT) is a newly developed therapy in which photon energy is converted into heat ($> 43^{\circ}\text{C}$) to kill tumor cells [1,2]. NIR-absorbing photothermal agents have been combined with a laser to use for treatment of the deep solid tumor [2,3]. With the assistance of photothermal agents in the solid tumor, the laser can penetrate deeply into tissues and destroy it, meanwhile neighboring healthy tissues can be protected against laser by reducing the scattered and absorbed photons [4,5]. With highly specific and minimally-invasiveness properties, PTT is a promising method for alternative treatment of cancer.

Recently photoacoustic imaging (PAI) has been developed as a novel imaging technique for cancer diagnostic and therapeutic monitoring purposes [6,7]. Photoacoustic agents have been used in PAI to enhance the contrast and specificity of imaging or target specific molecular processes [8,9]. Thus, PAI with the assistance of tumor-targeting nanoparticle platforms can accurately locate the tumor for the more-precisely guided PTT [10]. Taking the advantage of using the same wavelength laser, the near-infrared (NIR) photoabsorbers can be used for PAI-guided PTT.

Gold nanoparticles become the most commonly used photothermal

agent because of their unique surface plasmon resonance characteristic [11]. Among many gold structures, gold nanostars (AuNS) exhibit the excellent photothermal effect owing to the high molar extinction coefficient in NIR region (700 to 1870 nm) [12]. With the tips, AuNS have higher efficient heating in comparison to sphere nanostructure because the entering electric field penetrated easily into the tips and heat up whole gold matter [13,14]. Thus, AuNS are particularly suitable agents for PTT. Additionally, AuNS can also be used as a contrast agent for cancer diagnosis and therapeutic monitoring by PAI [15].

To synthesize AuNS, the seed-mediated or seedless methods are usually used [16,17]. Capping agents such as CTAB helps to achieve suitable morphology and size of nanoparticles [16]; however, toxicity issues remain. To overcome this issue, we have developed a novel method for the preparation of AuNS by using environmentally friendly materials. Chitosan (CS) was used as a stabilizer, vitamin C was used as a reducing agent, and water as a solvent for the one-step green synthesis of AuNS. Vitamin C is a good antioxidant derived from Citrus fruits and other vegetables, it can reduce the Au^{III} ion to Au^0 atom [18]. With good inherent properties such as highly positive charge, biodegradability, biocompatibility, nontoxicity, and low cost, CS is a preferred selection for enhancing the stability of unstable nanoparticles [19,20].

* Department of Biomedical Engineering, Pukyong National University, Busan 48513, Republic of Korea (J. Oh) and Department of Aero Mechanical Engineering, Jungwon University, Chungbuk 28024, Republic of Korea (S.-H. Ahn)

E-mail addresses: shahn@jwu.ac.kr (S.-H. Ahn), jungoh@pknu.ac.kr (J. Oh).

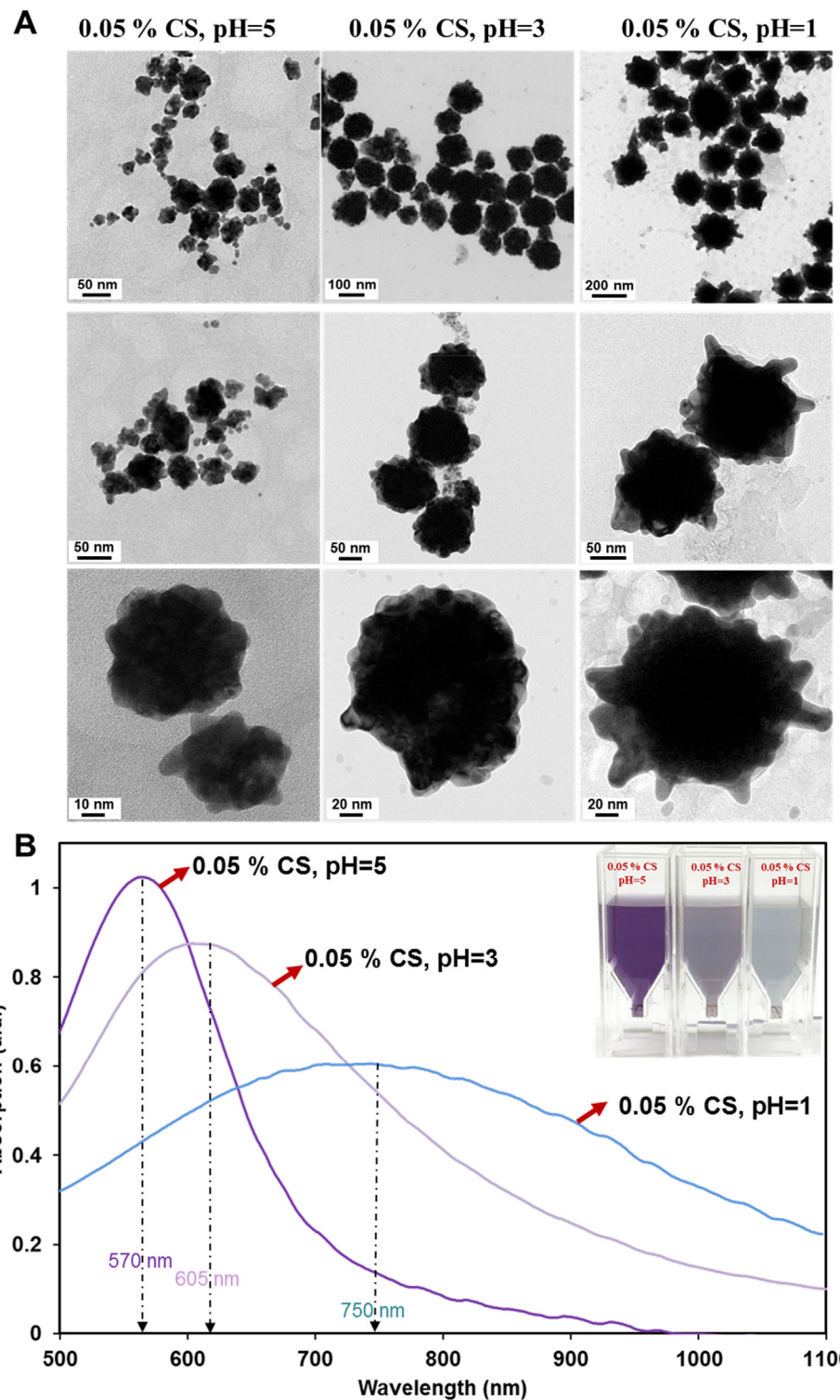


Fig. 1. (A) TEM of the Au nanoparticles at pH = 5, pH = 3 and pH = 1. (B) The corresponding UV-Vis absorption of Au nanoparticles solution.

Previous studies used CS for the synthesis of spherical gold nanoparticles, and the obtained product showed the high stability [21,22]. This is the first time, AuNS were successfully prepared with CS as a template and without any seeds or capping agents. Furthermore, we found that CS can also be a size-controllable agent for the synthesis of AuNS, and the size of resulted nanoparticles can be obtained in the range from 111 to 250 nm. The characterizations of AuNS were conducted and reported in details. The formation mechanism of AuNS was proposed to interpret mechanistic understanding. Subsequently, for

further biological applications, these AuNS were tested for biocompatibility, as well as photothermal cytotoxicity toward the normal and cancer cell models. The AuNS as good agents to enhance the photoacoustic imaging quality of tumors were also demonstrated by the *in vitro* PAI tests.

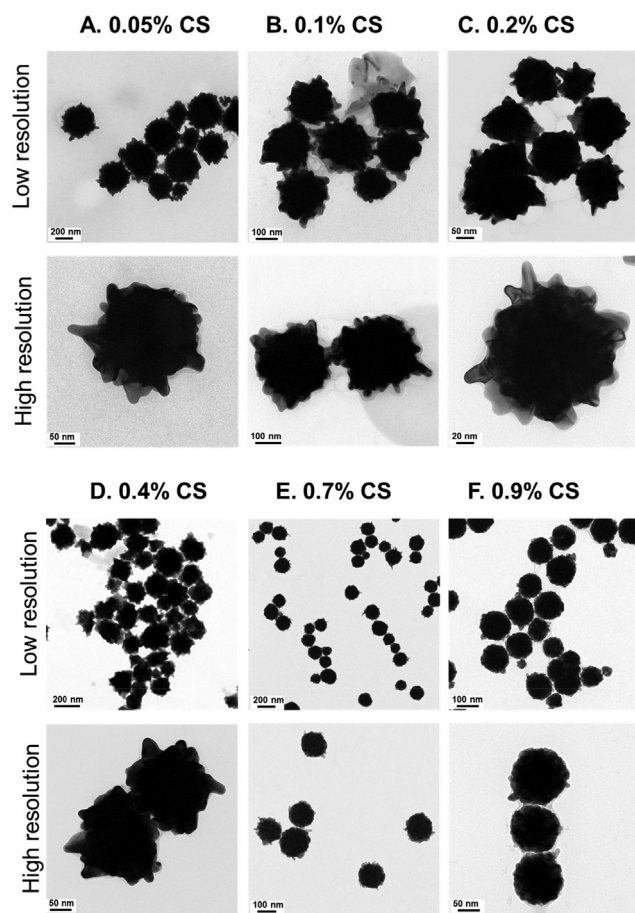


Fig. 2. TEM of synthesized AuNS from setups (different in concentration of CS).

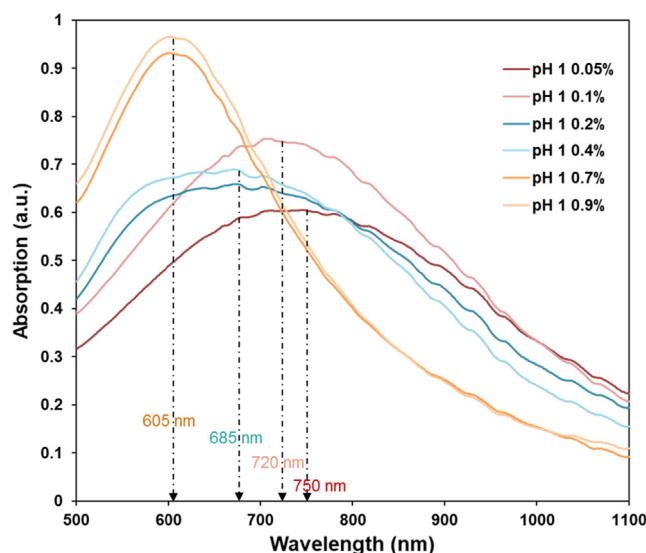


Fig. 3. UV-Vis absorption synthesized AuNS.

2. Materials and methods

2.1. Materials

CS (50 to 190 kDa, 75%–85% deacetylation), gold chloride ($\text{HAuCl}_4 \cdot 3\text{H}_2\text{O}$), L-ascorbic acid (vitamin C), hydrochloric acid (HCl, 37%), dimethyl sulfoxide (DMSO), 3-(4,5-dimethylthiazol-2-yl)-2,5-diphenyltetrazolium bromide (MTT), acridine orange (AO), and propidium

iodide (PI) were ordered from Sigma-Aldrich (St. Louis, MO, USA). The cell culture materials including Dulbecco's modified Eagle's medium (DMEM), fetal bovine serum (FBS), antibiotic, trypsin, and phosphate buffered saline (PBS) were bought from HyClone (South Logan, UT, USA).

2.2. One-step synthesis of AuNS

157.5 mg $\text{HAuCl}_4 \cdot 3\text{H}_2\text{O}$ was added to 25 mL DW in order to obtain HAuCl_4 0.01 M solution. Noted that to prepare a range of mass concentration (C%, w/v) of CS, the different amounts of CS were used. Firstly, the certain amount of CS and 20 mg vitamin C were added to 9 mL of distilled water containing baker. To CS completely dissolved in the solution, the stirring condition was kept for 4 h. Thereafter, 1 mL HAuCl_4 0.01 M was added to the obtained solution. After 3 min, the samples were centrifuged to collect the AuNS mass, then washing them three times with distilled water and dried in vacuum finally.

2.3. Characterization

The morphologies and lattice structures of samples were visualized at different magnification using a field-emission transmission electron microscopy (FETEM, JEOL JEM-2010 microscope, Japan). The absorption spectra of sample solutions were recorded by using a UV-Vis spectroscopy (Thermo Biomate 5 Spectrophotometer). The size distribution of samples was studied by an electrophoretic light scattering spectrophotometer (ELS-8000, OTSUKA Electronics Co. Ltd., Japan). The functional group's samples were characterized by the Fourier transform infrared spectroscopy (FTIR, Perkin Elmer Inc., USA). X-ray diffraction (XRD) analysis of the sample powder was performed with a Philips X'Pert-MPD diffractometer (Netherlands). An 808 nm NIR laser with continuous-wave (CW) pulse from Hi-Tech Optoelectronics Co. (Beijing, China) was used on all photothermal related experiments. Thermometer (MASTECH, CA, USA) was used to record temperature of irradiated solutions via a thermal fiber. A FLIR i5 infrared (IR) camera (Flirt Systems Inc., Portland, USA) was used to capture thermal photos.

2.4. Heating effect evaluation

The heating effect of prepared AuNS was evaluated by a photothermal conversion experiment. The cuvette containing 3 mL aliquot of 50 $\mu\text{g}/\text{mL}$ AuNS was directly laid under the laser fiber. Another cuvette containing PBS was used as a control. Thereafter, these cuvettes were continuously exposed to NIR laser with various power densities (0.5, 1.0, and 1.5 W/cm^2 , 5 min). All changes of the temperature of the irradiated samples were collected by thermometer; meanwhile, the thermal images were captured by IR camera every 1 min.

2.5. Cell line and cell culture condition

The breast cancer cell line MDA-MB-231 and the human osteosarcoma cell line MG-63 were purchased from Korea Cell Line Bank (Seoul, Korea). The DMEM media containing 10% FBS/1% antibiotic (v/v) was used to culture both cell lines. Cells were cultured on a 37 °C incubator containing a humidified 5% CO_2 /95% air atmosphere.

2.6. Cell uptake study

The MDA-MB-231 cells (2×10^5 cells/well) were seeded in a 6-well plate and cultured 24 h. Thereafter, the old media was removed and the media containing AuNS with various concentrations (15, 30, and 60 $\mu\text{g}/\text{mL}$) was added to each well. After further 12 h incubation, media with non-uptake AuNS were discarded and AuNS treated cells were washed three times with cold PBS. Then, the bright field and dark field images of AuNS incubated cells were immediately taken.

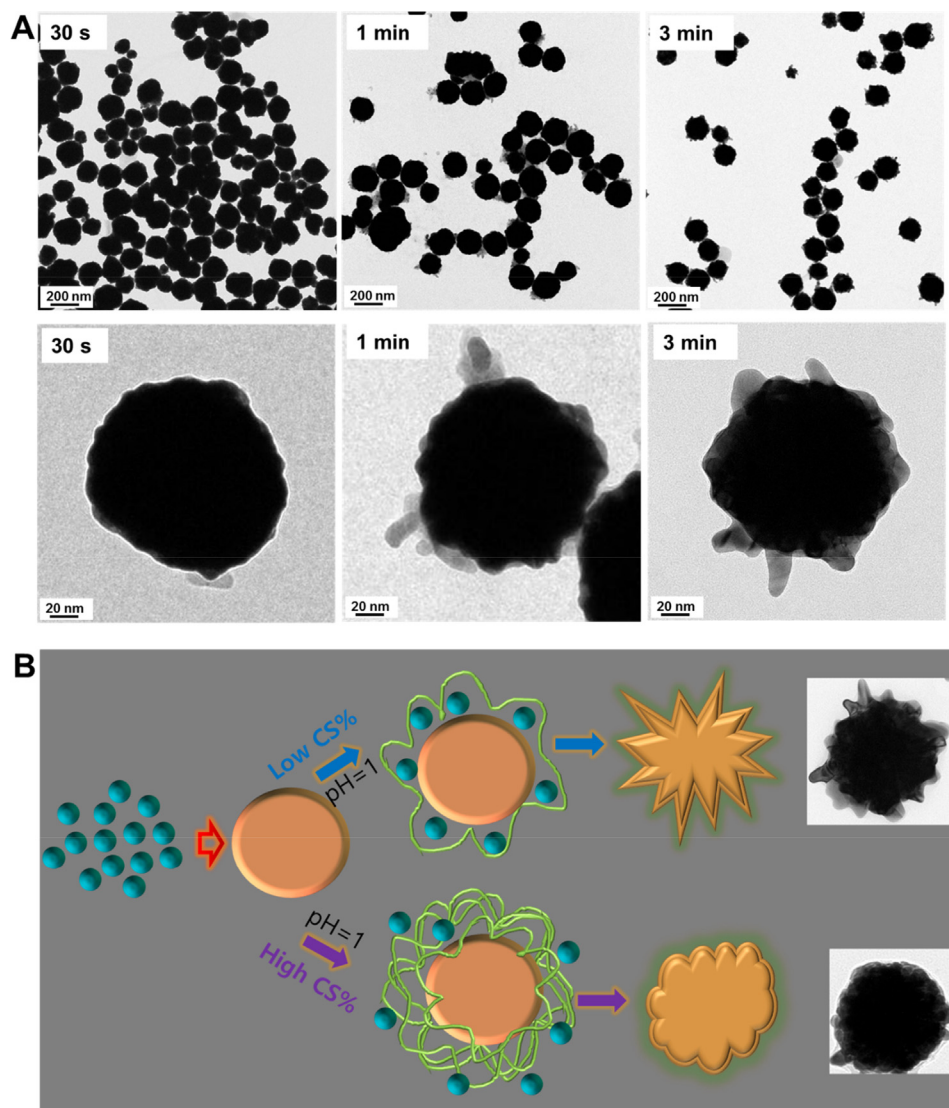


Fig. 4. (A) TEM images of gold nanoparticles after reacting for 30 s, 1 min, and 3 min (The reaction with 0.9% CS, pH = 1). (B) The proposed formation process of AuNS.

2.7. Biocompatibility study

A standard methyl thiazolyl tetrazolium (MTT) assay was used to evaluate the cell compatible property of AuNS. The MDA-MB-231 cells and MG-63 cells (1×10^4 cells/well) were seeded in 96-well plates and cultured for 24 h. Thereafter, old media were removed and 100 μ L media containing AuNS with different concentrations (0, 15, 30, 60, and 120 μ g/mL) was added to wells and incubated for 24 h. 100 μ L MTT was put to each well after further 24 h incubation. Then, 200 μ L DMSO was added to dissolve the formed formazan crystals. Subsequently, these 96-well plates were put in the plate reader to read the data at 570 nm wavelength.

To visualize the live/dead cells in the AuNS-treated cell dish, an AO/PI double staining was used. The nuclear of live cells emits the blue fluorescence by AO staining. Meanwhile, the nuclear of dead cells emits the red fluorescence by PI staining. The 6-well plate with a density of 2×10^5 cells/well was treated with three concentrations of AuNS solution (15, 30 and 60 μ g/mL) and incubated for 24 h. After staining with AO and PI, the fluorescent images of the cells were captured by a fluorescence microscope.

2.8. In vitro photothermal therapy

A density of 6×10^5 cells/well was seeded in the 6-well plate. The cells were gathered into four groups: control (no treatment, group I), NIR laser (group II), AuNS (group III), and AuNS plus NIR laser (group IV). A dose of 60 μ g/mL AuNS solution was added to cells in groups III and IV and incubated for 4 h. Then, cells in groups II and IV were illuminated with NIR laser (1.5 W/cm^2 , 5 min). To visualize the live/dead cells after the photothermal treatment, the AO/PI staining also was conducted. A mix solution of AO and PI was added to each well and the live/dead cells images were analyzed by a fluorescence microscope.

2.9. In vitro photoacoustic imaging

Based on the previous research [23], our PAI system used a Q-switched diode pumped solid-state laser (SPOT-10-100-532, Elforlight, UK) with a wavelength of 532 nm which operated at 5 kHz of repetition rate. The laser light was coupled into 50-m polarization-maintaining single mode fiber (PM-S405-XP, Nufern, USA) by fiber couplers and a variable beam splitter/attenuator. The output laser of two single mode fiber irradiated into the sample to generate PA signals with intensity energy under 13.3 mJ/cm^2 . An acoustic and optical beam combiner was

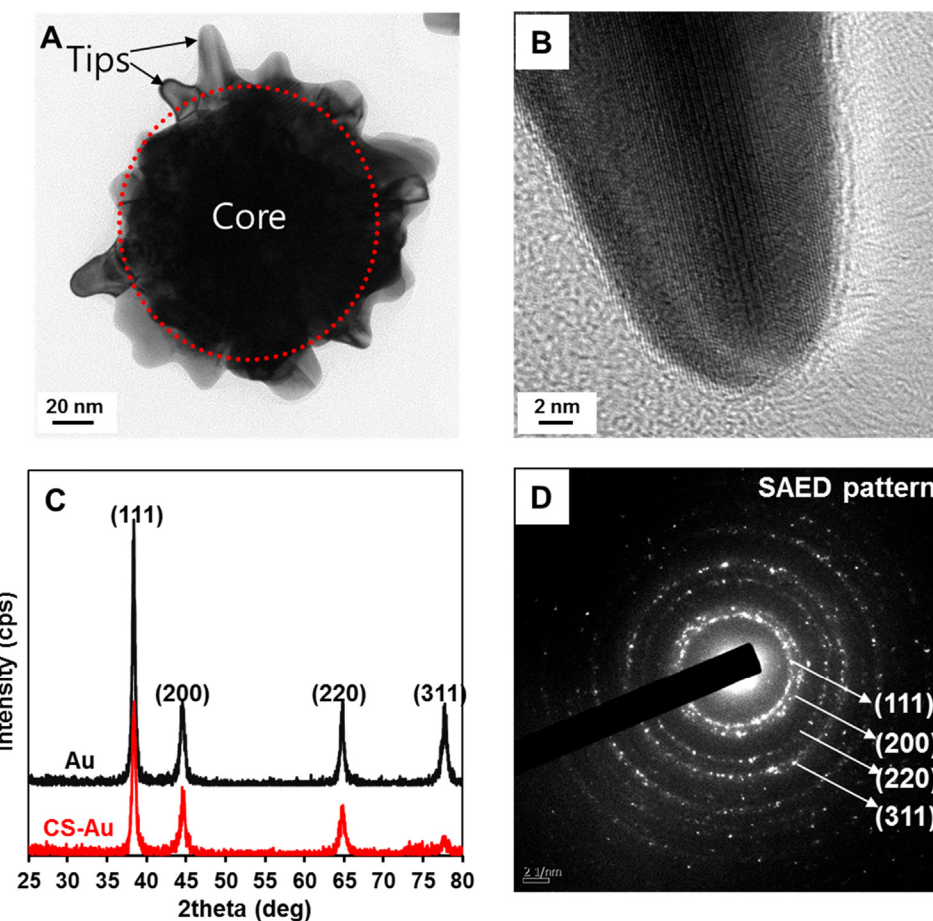


Fig. 5. (A, B) High-resolution TEM, (C) XRD, and (D) SAED analysis of AuNS.

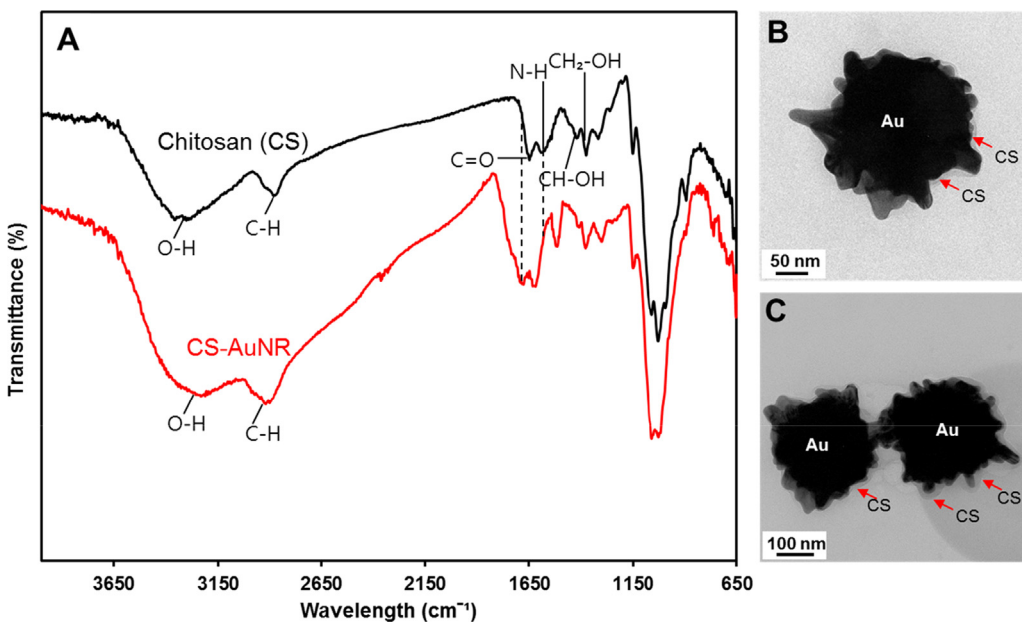
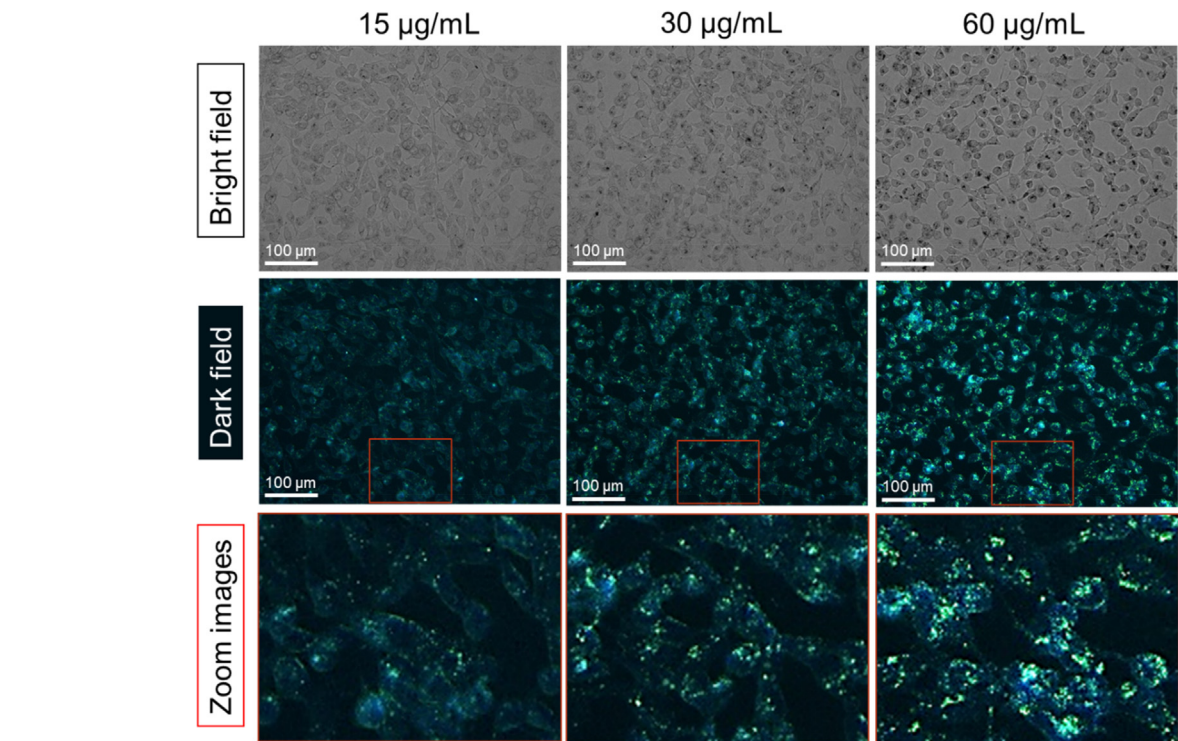
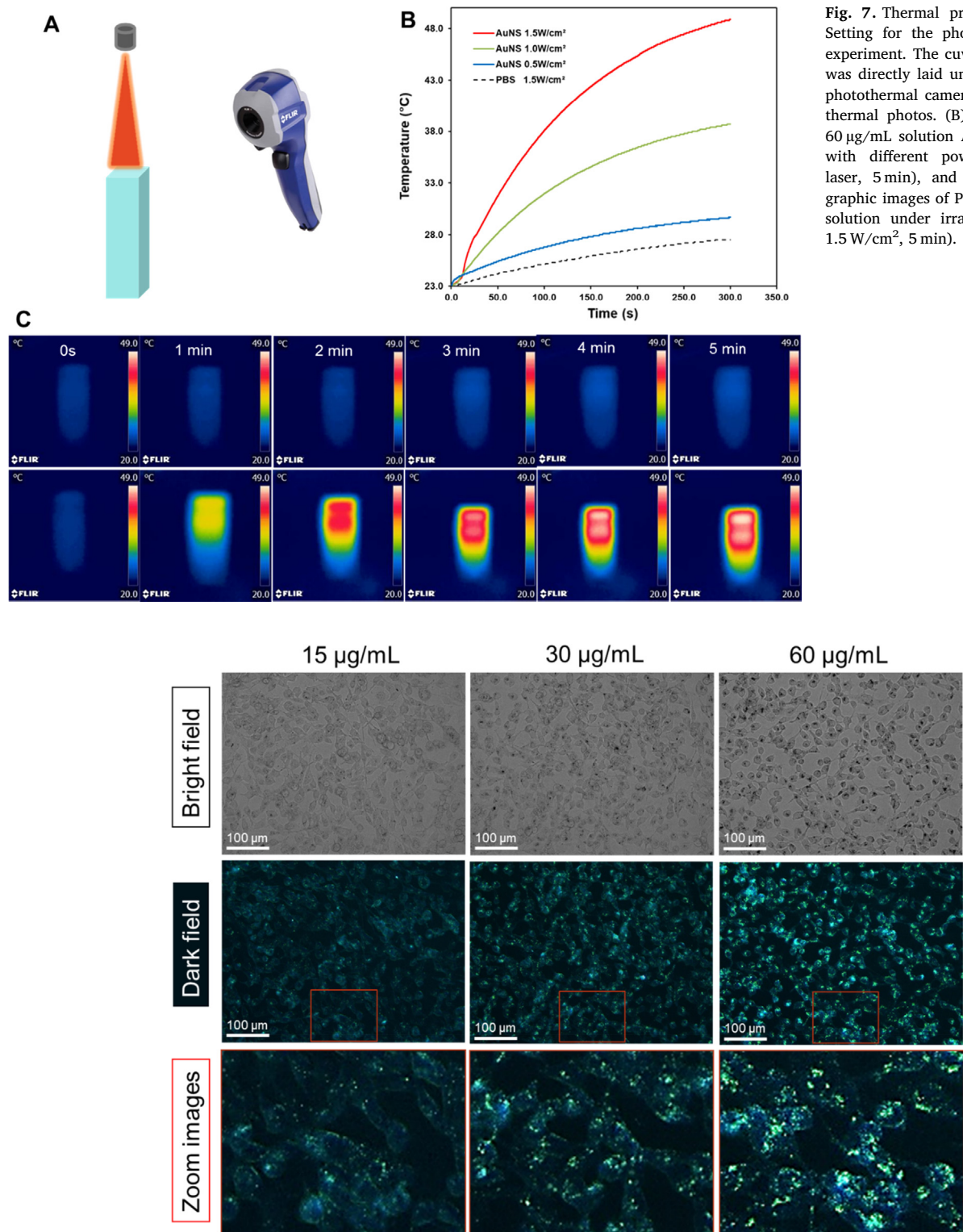


Fig. 6. (A) FTIR of CS and CS-stabilized AuNS, (B), and (C) TEM of CS-AuNS.

designed and fabricated to maximize the acquired PA signals. The three-axis linear stage in synchronization with the trigger from the laser enable to bi-directionally scan the OABC to get volumetric imaging. The generated PA signals were then picked up by an immersion transducer (V324-SM, Olympus, USA) with a center frequency of 25 MHz,

amplified by using two serially connected preamplifiers (ZFL-500LN, Mini-Circuits, USA), and finally acquired by a high-speed digitizer (NI PXI-5124, National Instruments, USA). The raw data were input to an offline process to reconstruct into PA images by MATLAB.

Various concentration solutions of AuNS (30, 15, 7.5, 3.75, 1.87,



and 0.93 µg/mL) were loaded to the PTFE tube (inner diameter 1.6 mm and the wall thickness 0.038 mm). Silicon was used to seal the ends of each tube, and the phantoms were placed in a degas water chamber for PAI.

3. Result and discussion

3.1. The role of pH on the formation of AuNS

CS with multiple reactive functional groups and excellent biocompatible can be as a stabilizer for gold structures and other nanoparticles [20,24]. Herein, we discovered that CS can be used as a template for the formation of AuNS in a single-step synthesis. CS is a

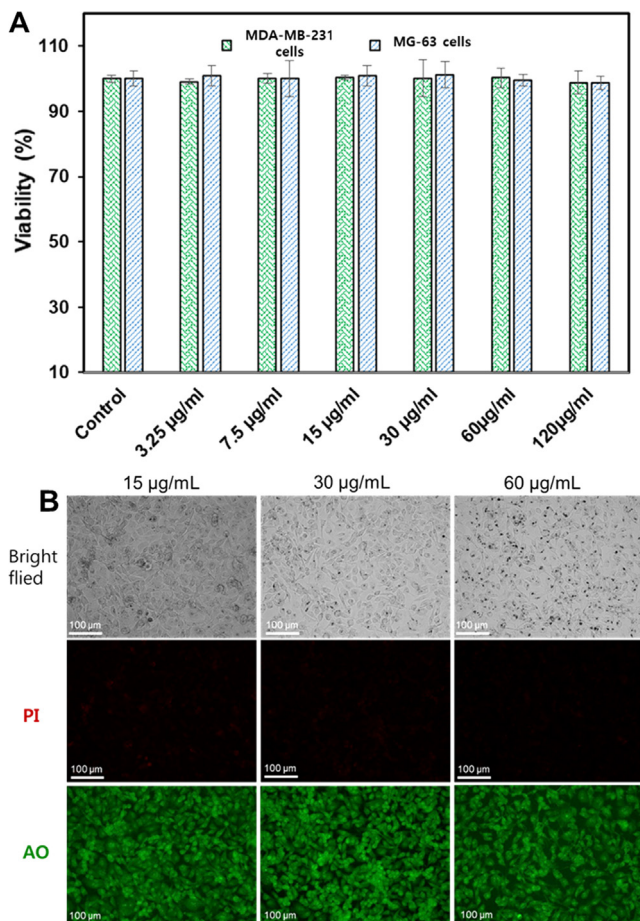


Fig. 9. (A) Cell viability of MDA-MB-231 cells and MG-63 cells treated with AuNS solutions (incubation time: 24 h). (B) Bright field and fluorescent images of MDA-MB-231 cells after 24 h incubation with AuNS.

linear marine-derived polymer of glucosamine and acetylglucosamine units that behave as a polyelectrolyte with highly positive charge density at low pH solutions [25]. So, changing the pH levels could effect on the behaviors and properties of CS. Low environmental pH increases the positive charge in CS. In order to evaluate the influence of pH on the formation of AuNS by using CS as a template, three experimental conditions with pH = 1, 3, and 5 were set with the fixed concentration of CS (0.05%, w/v). As shown in Fig. 1, gold structures with unclear tips were formed in the pH = 5 and pH = 3 solutions. The peak absorptions of resulted in gold solutions from pH = 5 and pH = 3 experiments were reached at about 570 nm and 605 nm, respectively, not in the NIR range. When the pH was adjusted to 1, the obtained gold solutions exhibited a well-defined star-like structure with a dense core and anisotropic tips. Because of star-like shape, AuNS had the strong absorption peak at 750 nm, which was extended into the NIR region.

3.2. Chitosan as a controllable nanoparticle size agent for the synthesis of AuNS

Six concentrations of CS from 0.05% to 0.9% (m/v) were set up to access the influence of CS concentrations on the formation of AuNS. As shown in Fig. 2, the TEM images revealed that the synthesized AuNS had differences in nanoparticles size and in morphology of tips. The synthesized AuNS at 0.05% (m/v) CS exhibited an average diameter of 225.9 ± 52.9 nm, those from CS 0.9% (m/v) had the mean diameter of 111.3 ± 56.2 nm. The CS amounts of 0.05% to 0.4% (m/v) resulted in the AuNS with elongated and sharp tips, meanwhile, the CS amounts of 0.7% to 0.9%, the tips of obtained AuNS were short and unsharp. The

UV-Vis absorption spectra (Fig. 3) revealed that the AuNS obtained from 0.05% to 0.4% (m/v) of CS experiments had the absorption peaks from 685 to 750 nm and strong broadband absorption in NIR region. However, the 0.7% to 0.9% (m/v) of CS experiments had an absorption peak at 605 nm and weak absorption in the NIR region. The AuNS with desired nanoparticles size and UV-Vis absorption peak can be prepared for different applications by controlling the CS concentration.

3.3. Proposed growth model of AuNS nanoparticles

The crystal structures of gold nanoparticles during the formation process were imaged at 30 s, 1 min, and 3 min by TEM (Fig. 4A). The core of the AuNS fully formed after 30 s. After 1 min, the tips partially grew on the surface of the core. After 3 min, the tips of AuNS completely grown. Based on the data from TEM, the growing process of AuNS was proposed through 2 stages. At the first stage, the Au^{III} ion was quickly reduced to Au^0 atom by vitamin C. After the concentration of Au^0 atoms reached supersaturating status, they began to nucleate and form the core of AuNS [26]. At the second stage, CS with highly positive charges could bind to the core via a strong interaction with Au nuclei. The negative AuCl^- bound to the positive CS, and the tips starting to grow at the loose contact points of CS and the core, facilitating the anisotropic growth of gold nanostructures. In the solution with a high concentration of CS, the CS quickly bound on the surface of the core and fully cover it, blocking the contact of AuCl^- and the core, leading to the unsuccessful formation of the tips. The proposed formation process of AuNS was presented in Fig. 4B.

From the proposed formation process of AuNS, the effect of pH on the formation of nanostar can be hypothesized. With the highly positive charge (at pH = 1), CS can quickly bind to the core of Au nanoparticles and have an effect the formation of the tips. When the negative AuCl^- bound to the CS, the tips started to grow at the loose contact points of CS and the core, facilitating the anisotropic growth of gold nanostructures and resulting a well-defined star-like structure. When pH = 3 or pH = 5, the CS was not highly positive charge and did not bind quickly to the nuclear. So, the nuclear grew without the orientation of CS and the AuNS was not successfully formed.

3.4. Characterization of AuNS

3.4.1. High-resolution TEM, SAED, and XRD

From high-resolution TEM (Fig. 5A), the core and the tips of the AuNS can be distinguished clearly. XRD was used to identify the crystal structure of pure Au nanoparticles and CS stabilized-AuNS. The XRD data pattern of pure Au nanoparticles (Fig. 5C) exhibited peaks with high intensity at approximately 38.1° , 44.3° , 64.5° , and 77.7° , which correspond to the (1 1 1), (2 0 0), (2 2 0), and (3 1 1) planes face-centered cubic (fcc) metal crystals, respectively. The XRD pattern of CS stabilized-AuNS displayed the same peaks, however, the intensity of four peaks, was reduced in comparison with one of the bare AuNS, especially the peak at 77.7° . The decreasing in XRD intensity caused by the presence of CS on the surface of AuNS. The SAED pattern also confirmed the crystalline structure of Au nanoparticles with the (1 1 1), (2 0 0), (2 2 0), and (3 1 1) crystals planes (Fig. 5C).

3.4.2. FT-IR analysis

The FTIR of CS and CS-stabilized AuNS were analyzed and presented in Fig. 6. The characterized peaks of CS can be seen on the spectrum, shown in Fig. 6A. Particularly, the broadband of $3292\text{--}3352\text{ cm}^{-1}$ related to O-H stretching, and the intramolecular hydrogen bonds. The C-H stretch of the alkyl groups was defined by the vibrational band between 2916 and 2870 cm^{-1} . The peaks at 1646 cm^{-1} and 1374 cm^{-1} associated with C=O stretching of amide I and C-N stretching of amide III, respectively [27,28]. N-H bending of amide II and I were characterized by the two small peaks at 1550 cm^{-1} and 1581 cm^{-1} , respectively [29].

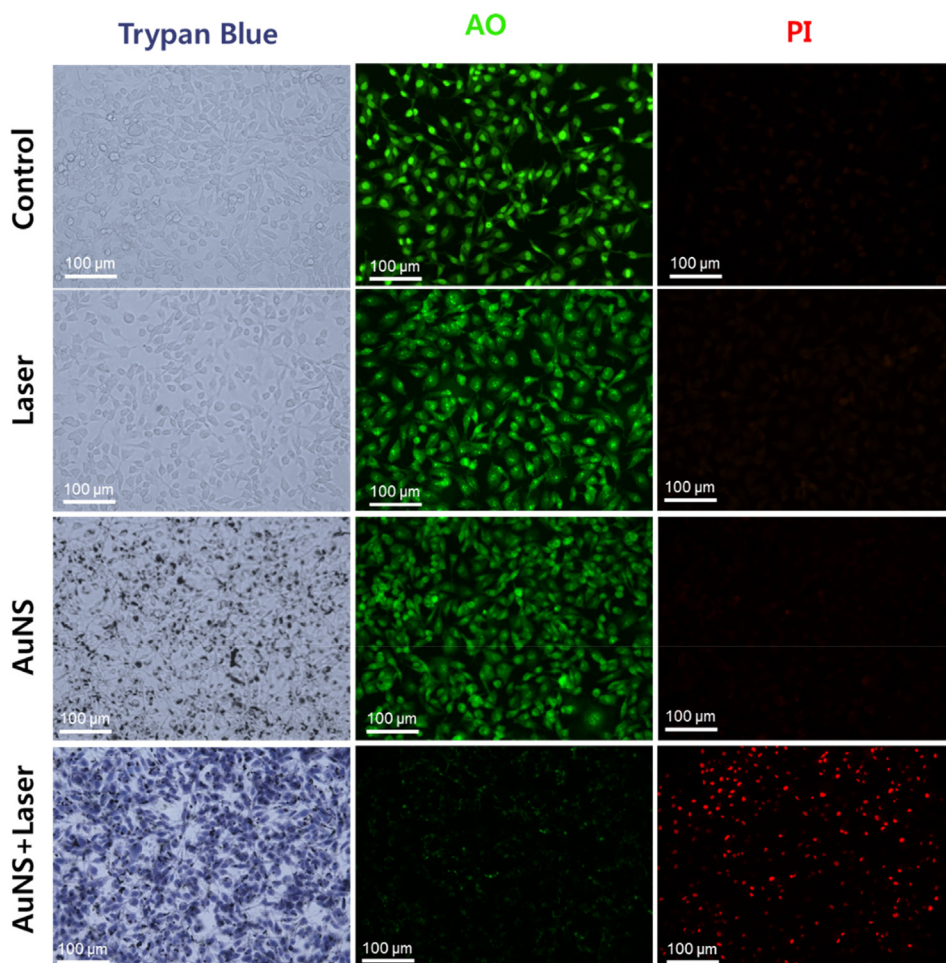


Fig. 10. Trypan blue and AO/PI staining of MDA-MB-231 cells of control group and treated groups: NIR laser only (1.5 W/cm^2 , 5 min), 60 $\mu\text{g/mL}$ AuNS, and 60 $\mu\text{g/mL}$ AuNS plus NIR laser (1.5 W/cm^2 , 5 min). (For interpretation of the references to colour in this figure legend, the reader is referred to the web version of this article.)

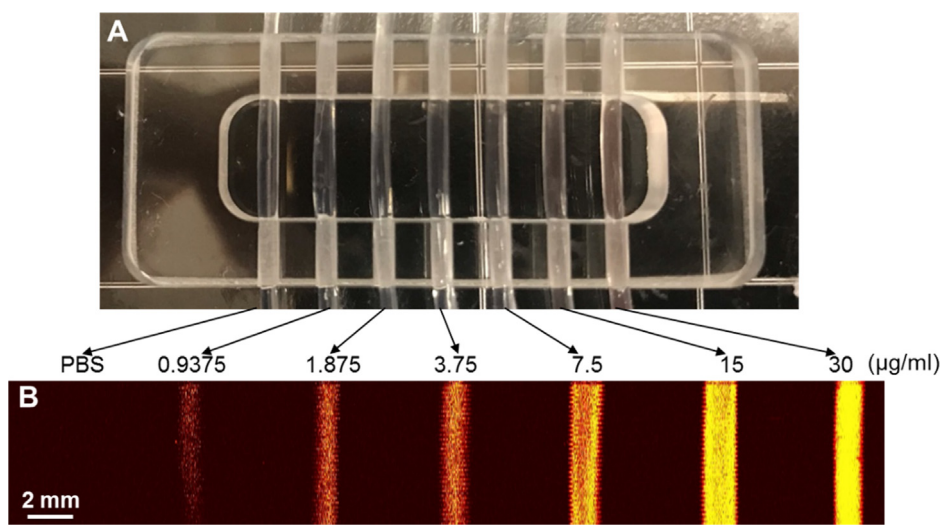


Fig. 11. PAI experiment. (A) The PTFE tubes containing the AuNS with different concentrations. (B) The corresponding PA signals.

In the spectrum of CS-stabilized AuNS, the characterized functional groups of CS were observed clearly, determining the presence of CS on the surface of AuNS (Fig. 6A). Particularly, typical C–H stretch vibrations of CS were found at 2977 and 2899 cm^{-1} peak; bending vibrations of hydroxyls groups were characterized by the 1231 cm^{-1} peak. Two

peaks at 1541 and 1508 cm^{-1} related to the C=O stretching of amide II; the peaks around 950 and 1048 cm^{-1} related to the saccharide units of CS. Especially, the peaks at 1657 cm^{-1} and 1600 cm^{-1} , corresponding to CS $-\text{CONH}_2$ and $-\text{NH}_2$ groups of CS, disappeared and a new band at 1635 cm^{-1} appeared, which indicated the interaction of

AuNS and the nitrogen atom of CS.

The presence of CS on the surface of AuCS can be clearly observed by high-resolution TEM images (Fig. 6B, C). Besides improving the biocompatible of AuNS [19], the cover of CS can help the AuNS in conjugation with tumor targeting ligand or anticancer drugs [20].

3.5. Photothermal performance of AuNS

3.5.1. Photothermal behavior of AuNS

To evaluate the potential of AuNS as photothermal agents for therapeutic purpose, AuNS obtained from 0.4% CS experiment was evaluated with regard to their photothermal effect. The temperature changes of the irradiated samples were plotted against the duration of time and shown in Fig. 7B. Under NIR irradiation (NIR laser, 1.5 W/cm²), the temperature of 60 µg/mL AuNS solution increased up to 48.5 °C after 5 min; whereas about 4 °C increment can be obtained for PBS. To clarify the heating efficiency of AuNS, the cuvette containing AuNS and cuvette containing PBS were illuminated under the same condition (NIR laser, 1.5 W/cm²). From the above results, AuNS revealed their potential as a promising photothermal agent for PTT.

3.5.2. Uptake of AuNS on the cancer cell

Taking advantage of the plasmonic properties of gold nanoparticles, we used the dark field (DF) microscopy to detect the uptake of AuNS by the MDA-MB-231 cells. The dark field images showed clearly the presence of AuNS inside the MDA-MB-231 cells (Fig. 8). When the concentration of AuNS was increased, the brighter image was taken. With the highly positive charges of the CS layer, the AuNS could easily attach and pass through the membrane of the cancer cells.

3.5.3. The biocompatibility of AuNS

Cell compatibility is an important property of photothermal agents for the biomedical application. Standard MTT assay was used to evaluate the biocompatibility of AuNS. After 24 h, the viability of both of AuNS-incubated MDA-MB-231 cells and AuNS-incubated MG-63 cells were still around 100%, even at a dose of 120 µg/mL AuNS solution (Fig. 9A). The fluorescent images of the cells taken after AO/PI staining were shown in Fig. 9B and Fig. S4 (Supporting Information); in those, no dead cells could be observed. The results demonstrated that the synthesized AuNS is the good biocompatible materials.

3.5.4. Cell-killing effect of AuNS plus NIR laser

Motivated by highly efficient conversion of absorbed photons to heat using AuNS plus NIR laser, we further investigated the *in vitro* PTT of MDA-MB-231 breast cancer cells. The cells were divided into four groups: control (no treatment, group I), NIR laser (group II), AuNS (group III), and AuNS plus NIR laser (group IV). During the laser illumination of the AuNS-treated cells sample, thermographic images of solution was captured every 1 min and presented in Fig. S5 (Supporting Information). The temperature of AuNS-treated cells sample was reached to 50 °C after 5 min. Two different staining methods were used to analyze the *in vitro* PTT effect of AuNS on the MDA-MB-231 cells (Fig. 10). The first method is trypan blue staining; the dead and damaged cells are the blue cells. The second one is AO/PI staining; the green fluorescent cells are the live cells and the red ones are the dead cells. In the first column of Fig. 10, the cells on groups I, II, and III were not stained by trypan blue; meanwhile, all the cells in group IV were blue. With the AO/PI staining, the same outcomes were observed. Particularly, most of the cells in group IV emitted the red fluorescence, and the cells of the remaining groups emitted the green fluorescence. These results demonstrated that a single treatment with NIR laser or AuNS could not destroy the cancer cells. When the NIR laser was combined with AuNS, the treatment was highly effective. When the cell dish was partially illuminated with a laser spot, the borderline between unstained and stained trypan blue was obviously seen, as shown in Fig. S6 (Supporting Information). These experimental findings proved that

AuNS could act as an effective NIR photoabsorber to destroy the tumor cells *in vitro*.

3.6. Photoacoustic performance of AuNS

AuNS can accumulate in the tumor through passive cellular uptake which bases on enhanced permeability and retention effect or via positive cellular uptake which bases on receptor-ligand interactions using tumor-targeting ligand-conjugated AuNS [30]. Thus, PA imaging with the assistance of AuNS can be used to detect many types of tumors. Additionally, owing to the broadband absorption of AuNS, we can use the laser with different wavelengths to obtain the PA imaging.

PAI is an emerging imaging modality with non-invasive properties and can be used to guide PTT. In this study, our designed PAI system was used to acquire the PA images of AuNS. The setup of PAI system was presented in Fig. S7 (Supporting Information). The PTFE tubes containing AuNS displayed strong PA signals with increasing magnitude when AuNS concentration increased; oppositely, the control tube with PBS did not emit any PA signals (Fig. 11B). Therefore, AuNS can become good agents to enhance the PA imaging quality of tumors as demonstrated by the *in vitro* PAI results.

4. Conclusion

This study put efforts for the new method to synthesize AuNS with environmental materials; in that, the vitamin C as green reducing agent and CS as a shape directing-agent were used. These obtained AuNS have a size from 111 to 250 nm and different peak absorptions. The CS can be used to achieve the AuNS with a desired size and suitable UV-Vis absorption peak for different applications. The produced AuNS were characterized with TEM, SAED, XRD, FTIR, DLS, and examined for their effectiveness on *in vitro* PTT and PAI. The synthesized AuNS not only showed highly photothermal stability, high absorption in the NIR region, but also exhibited the excellent biocompatibility on both MDA-MB-231 and MG-63 cells. The effectively killing MDA-MB-231 cancer cells by AuNS plus NIR laser, proved their ability for PTT. Furthermore, the strong PA signals of the AuNS also confirmed the promising of AuNS-based PAI.

Acknowledgements

This research was supported by a grant from the Marine Biotechnology Program (20150220) funded by the Ministry of Oceans and Fisheries, Republic of Korea.

Data availability

The raw/processed data required to reproduce these findings cannot be shared at this time due to legal or ethical reasons.

Appendix A. Supplementary material

Supplementary data to this article can be found online at <https://doi.org/10.1016/j.eurpolymj.2019.06.023>.

References

- [1] X. Huang, M.A. El-Sayed, Plasmonic photo-thermal therapy (PPTT), *Alexandria J. Med.* 47 (1) (2011) 1–9.
- [2] T.T.V. Phan, N. Quang Bui, S.-W. Cho, S. Bharathiraja, P. Manivasagan, S. Moorthy, S. Mondal, C.-S. Kim, J. Oh, Photoacoustic imaging-guided photothermal therapy with tumor-targeting HA-FeOOH@PPy, *Nanorods* (2018).
- [3] D. Jaque, L. Martínez Maestro, B. del Rosal, P. Haro-Gonzalez, A. Benayas, J.L. Plaza, E. Martín Rodríguez, J. García Solé, *Nanoscale* 6 (16) (2014) 9494–9530.
- [4] T.T.V. Phan, N.Q. Bui, M.S. Moorthy, K.D. Lee, J. Oh, Synthesis and *in vitro* performance of polypyrrole-coated iron-platinum nanoparticles for photothermal therapy and photoacoustic imaging, *Nanoscale Res. Lett.* 12 (1) (2017) 570.

- [5] S. Hwang, J. Nam, S. Jung, J. Song, H. Doh, S. Kim, Gold nanoparticle-mediated photothermal therapy: current status and future perspective, *Nanomedicine* 9 (13) (2014) 2003–2022.
- [6] M. Xu, L.V. Wang, Photoacoustic imaging in biomedicine, *Rev. Sci. Instrum.* 77 (4) (2006) 041101.
- [7] L.V. Wang, J. Yao, A practical guide to photoacoustic tomography in the life sciences, *Nat. Methods* 13 (8) (2016) 627–638.
- [8] J. Weber, P.C. Beard, S.E. Bohndiek, Contrast agents for molecular photoacoustic imaging, *Nat. Methods* 13 (2016) 639.
- [9] T.T.V. Phan, S. Bharathiraja, V. Tu Nguyen, S. Moorthy, P. Manivasagan, K. Dae Lee, J. Oh, Polypyrrole–methylene blue nanoparticles as a single multifunctional nanoplatform for near-infrared photo-induced therapy and photoacoustic imaging, *RSC Adv.* 7 (56) (2017) 35027–35037, <https://doi.org/10.1039/C7RA02140B>.
- [10] L.V. Wang, Multiscale photoacoustic microscopy and computed tomography, *Nat. Photonics* 3 (9) (2009) 503–509.
- [11] X. Huang, M.A. El-Sayed, Gold nanoparticles: Optical properties and implementations in cancer diagnosis and photothermal therapy, *J. Adv. Res.* 1 (1) (2010) 13–28.
- [12] C.G. Khoury, T. Vo-Dinh, Gold Nanostars For Surface-Enhanced Raman Scattering: Synthesis, Characterization and Optimization, *The journal of physical chemistry, C, Nanomater. Interfaces* 2008 (112) (2008) 18849–18859.
- [13] G. Baffou, R. Quidant, C. Girard, Heat generation in plasmonic nanostructures: Influence of morphology, *Appl. Phys. Lett.* 94 (15) (2009) 153109.
- [14] F. Hao, C.L. Nehl, J.H. Hafner, P. Nordlander, Plasmon resonances of a gold nanostar, *Nano Letters* 7 (3) (2007) 729–732.
- [15] M.S. Moorthy, S. Bharathiraja, P. Manivasagan, Y. Oh, T.T.V. Phan, S. Mondal, H. Kim, K.D. Lee, J. Oh, Synthesis of Fe 3 O 4 modified mesoporous silica hybrid for pH-responsive drug delivery and magnetic hyperthermia applications, *J. Porous Mater.* 25 (4) (2018) 1251–1264.
- [16] H.-Y. Wu, M. Liu, M.H. Huang, Direct synthesis of branched gold nanocrystals and their transformation into spherical nanoparticles, *J. Phys. Chem. B* 110 (39) (2006) 19291–19294.
- [17] O.M. Bakr, B.H. Wunsch, F. Stellacci, High-yield synthesis of multi-branched urchin-like gold nanoparticles, *Chem. Mater.* 18 (14) (2006) 3297–3301.
- [18] B. Zümreoglu-Karan, A rationale on the role of intermediate Au(III)–vitamin C complexation in the production of gold nanoparticles, *J. Nanopart Res.* 11 (5) (2009) 1099–1105, <https://doi.org/10.1007/s11051-008-9498-5>.
- [19] P. Manivasagan, S. Bharathiraja, M. Santha Moorthy, S. Mondal, T. Nguyen, H. Kim, T. Phan, K. Lee, J. Oh, Biocompatible Chitosan oligosaccharide modified gold nanorods as highly effective photothermal agents for ablation of breast cancer cells, *Polymers* 10 (3) (2018) 232.
- [20] T.T.V. Phan, M.S. Moorthy, H.W. Kang, S.Y. Nam, Y.W. Lee, J. Oh, Coating Chitosan thin shells: a facile technique to improve dispersion stability of magnetoliposomes, *J. Nanosci. Nanotechnol.* 18 (1) (2018) 583–590.
- [21] H. Huang, X. Yang, Synthesis of polysaccharide-stabilized gold and silver nanoparticles: a green method, *Carbohydr. Res.* 339 (15) (2004) 2627–2631.
- [22] H. Huang, Q. Yuan, X. Yang, Preparation and characterization of metal–chitosan nanocomposites, *Colloids Surf. B Biointerfaces* 39 (1) (2004) 31–37.
- [23] N.Q. Bui, S.-W. Cho, M.S. Moorthy, S.M. Park, Z. Piao, S.Y. Nam, H.W. Kang, C.-S. Kim, J. Oh, In vivo photoacoustic monitoring using 700-nm region Raman source for targeting Prussian blue nanoparticles in mouse tumor model, *Sci. Rep.* 8 (1) (2018) 2000.
- [24] T.T.V. Phan, G. Hoang, V.T. Nguyen, T.P. Nguyen, H.H. Kim, S. Mondal, P. Manivasagan, M.S. Moorthy, K.D. Lee, O. Junghwan, Chitosan as a stabilizer and size-control agent for synthesis of porous flower-shaped palladium nanoparticles and their applications on photo-based therapies, *Carbohydr. Polym.* 205 (2019) 340–352.
- [25] B. Bellich, I. D'Agostino, S. Semeraro, A. Gamini, A. Cesàro, “The Good, the Bad and the Ugly” of Chitosans, *Mar. Drugs* 14 (5) (2016) 99.
- [26] C. Burda, X. Chen, R. Narayanan, M.A. El-Sayed, Chemistry and properties of nanocrystals of different shapes, *Chem. Rev.* 105 (4) (2005) 1025–1102.
- [27] A.B. Vino, P. Ramasamy, V. Shanmugam, A. Shanmugam, Extraction, characterization and in vitro antioxidative potential of chitosan and sulfated chitosan from Cuttlebone of Sepia aculeata Orbigny, 1848, *Asian Pacific J. Trop. Biomed.* 2 (1, Supplement) (2012) S334–S341.
- [28] C. Song, H. Yu, M. Zhang, Y. Yang, G. Zhang, Physicochemical properties and antioxidant activity of chitosan from the blowfly Chrysomya megacephala larvae, *Int. J. Biol. Macromol.* 60 (2013) 347–354.
- [29] S.-H. Lim, S.M. Hudson, Synthesis and antimicrobial activity of a water-soluble chitosan derivative with a fiber-reactive group, *Carbohydr. Res.* 339 (2) (2004) 313–319.
- [30] H. Norouzi, K. Khoshgard, F. Akbarzadeh, In vitro outlook of gold nanoparticles in photo-thermal therapy: a literature review, *Lasers Med. Sci.* 33 (4) (2018) 917–926.